Nanoscale surface pattern formation kinetics on germanium irradiated by Kr^+ ions

Eitan Anzenberg,[1] Joy C. Perkinson,[2] Charbel S. Madi,[2] Michael J. Aziz,[2] and Karl F. Ludwig, Jr.[1]
[1]*Department of Physics, Boston University, Boston Massachusetts 02215, USA*
[2]*Harvard School of Engineering and Applied Sciences, Cambridge Massachusetts 02138, USA*
(Received 17 July 2012; published 13 December 2012)

Nanoscale surface topography evolution on Ge surfaces irradiated by 1 keV Kr^+ ions is examined in both directions perpendicular and parallel to the projection of the ion beam on the surface. Grazing incidence small angle x-ray scattering is used to measure *in situ* the evolution of surface morphology via the linear dispersion relation. A transition from smoothing (stability) to pattern-forming instability is observed at a critical ion incidence angle of approximately 62° with respect to the surface normal. The linear theory quadratic coefficients which determine the surface stability/instability are determined as a function of bombardment angle. The Ge surface evolution during Kr^+ irradiation is qualitatively similar to that observed for Ar^+ irradiation of Si. However, in contrast to the case of Si under Ar^+ irradiation, the critical angle separating stability and instability for Ge under Kr^+ irradiation cannot be quantitatively reproduced by the simple Carter-Vishnyakov mass redistribution model.

DOI: 10.1103/PhysRevB.86.245412 PACS number(s): 68.49.Sf, 81.16.Rf, 81.65.Cf

Uniform ion irradiation of solid surfaces can cause ultrasmoothing[1,2] or self-organized nanoscale surface topographic pattern formation, depending on control parameters such as ion and target species, ion energy and incidence angle, target temperature, and surface impurity coverage.[2–14] Patterning as small as 7 nm[15] has created interest in the potential use of ion bombardment as a sublithographic nanofabrication technique. Understanding the mechanisms behind nanopatterning during ion bombardment remains an important goal.

Models have shown that surface instabilities can arise from the curvature dependence of sputter erosion[16,17] or of impact-induced mass redistribution.[18] Pattern formation arises when a destabilizing process such as one of these occurs simultaneously with a stabilizing process that has a different dependence on wave number q, such as surface diffusion[17–19] or surface-confined viscous flow.[20,21] These effects have been unified into a parameter-free theory by Norris *et al.* [22,23] that predicts pattern formation, or the lack thereof, based on input from molecular dynamics simulations of craters produced by individual ion impacts.

Experimental studies of noble gas ion bombardment of Si at room temperature found that below a critical incident ion angle $\theta_c \cong 45°$ with respect to the surface normal, the surface is smoothened by ion bombardment.[2,12,18,24,25] Above this critical angle, the surface forms parallel-mode ripples, in which the wave vector is parallel to the projection of the ion beam on the surface.. Recently we have used *in situ* grazing-incidence small-angle x-ray scattering (GISAXS) to quantitatively measure the Si surface time evolution above and below θ_c in both the directions parallel to the projection of the ion beam on the surface (x direction)[26] and the perpendicular surface direction (y direction).[24] These studies were the first to quantitatively compare the erosive and redistributive contributions in an isotropic material. They concluded that impact-induced mass redistribution was the dominant cause of stability or instability, and that the effect of curvature-dependent sputtering is an order of magnitude smaller, except possibly at the most grazing incidence angles. The simple Carter-Vishnyakov (CV) model for impact-induced mass redistribution provided quantitative agreement with the observed smoothing rate in perpendicular modes and the rate and observed angular dependence in parallel modes, including the value $\theta_c \cong 45°$. The same conclusion arose from the crater-function theory of Norris *et al.*[23] using input parameters derived from molecular dynamics simulations.

While the experimental studies showed that the CV model, with surface-confined viscous flow replacing surface diffusion as the stabilizing process, accurately described the kinetics of smoothing and pattern formation in parallel and perpendicular modes for Si under low-energy Ar^+ bombardment, it is not yet known how broad the validity of this model is, even within the restricted category of monatomic semiconductors. Therefore we here present an analogous experimental study of ion bombardment of Ge by 1 keV Kr^+ ions.

A linear stability analysis of a flat, isotropic, monatomic surface undergoing ion bombardment while simultaneously relaxing by surface-confined viscous flow yields the following early time evolution of surface topography:

$$\frac{\partial h(\boldsymbol{q},t)}{\partial t} = -\left[S_x(\theta)q_x^2 + S_y(\theta)q_y^2 + B\left(q_x^2+q_y^2\right)^2\right]h(\boldsymbol{q},t) + \xi(\boldsymbol{q},t), \quad (1)$$

where $h(\boldsymbol{q},t)$ is the Fourier transform of the surface height $h(x,y)$ at time t, $S_{x,y}$ are the θ-dependent kinetic curvature coefficients causing surface instability (stability) when negative (positive), $\xi(\mathbf{q},t)$ is the Fourier transform of a stochastic noise term reflecting the random nature of the ion irradiation process, and $B = \gamma d^3/3\eta$ is the coefficient of surface-confined viscous flow in the $qd \ll 1$ limit,[21] where γ is the surface free energy,η is the viscosity of the ion-stimulated layer during irradiation, and d is the thickness of the viscous layer. Solving Eq. (1) for the ensemble-averaged height-height structure factor $\langle S(\mathbf{q},t)\rangle = \langle h(\mathbf{q},t)h^*(\mathbf{q},t)\rangle$ yields

$$\langle S(\mathbf{q},t)\rangle = \left[S(\mathbf{q},0) + \frac{\alpha}{2R(\mathbf{q})}\right]\exp[2R(\mathbf{q})t] - \frac{\alpha}{2R(\mathbf{q})}, \quad (2)$$

where $S(\mathbf{q},0)$ is the structure factor of the sample at time $t = 0$, α is the structure factor of the stochastic white noise, and $R(\mathbf{q})$

is the linear dispersion relation given by

$$R(\mathbf{q}) = -S_x(\theta)q_x^2 - S_y(\theta)q_y^2 - B\left(q_x^2 + q_y^2\right)^2. \qquad (3)$$

Positive $R(\mathbf{q})$ amplifies fluctuations, causing an instability at wave vector $\mathbf{q}$, whereas negative $R(\mathbf{q})$ damps fluctuations and stabilizes fluctuations at wave vector $\mathbf{q}$.

In this study we use GISAXS to characterize the evolution of surface height-height correlations *in situ* during ion bombardment. In the Born approximation for small height fluctuations the GISAXS scattering pattern is proportional to the structure factor $\langle S(\mathbf{q},t)\rangle$.

For the GISAXS experiments, prerippled and presmoothened samples were first prepared off-site in an ultrahigh vacuum chamber with a base pressure of 2.2×10^{-8} Torr. For these preparatory treatments, samples measuring 1×1 cm^2 were cleaved from Ge(001) (p-type, 0.4 Ω cm) and were affixed using molten indium to graphite wedges shielded everywhere by silicon wafers to minimize contamination by metallic impurities. Wedges' surface normals were at angles of 0° and 60° with respect to the ion source. Samples were then uniformly irradiated by 500 eV Kr^+ ions using a Veeco RF source with 3 cm graphite grids at room temperature and a pressure of 1.8×10^{-4} Torr. The distance from the ion source to the sample was 15 cm. Self-organized ripple structures formed on sample surfaces irradiated at 60°, whereas the surfaces of samples irradiated at 0° were smoothed. All samples develop a thin amorphous surface layer during ion bombardment; the thickness of the amorphous layer is approximately equal to the penetration depth of the atomic collision cascades caused by the ion beam. Using atomic force microscopy and scanning electron microscopy we observe no evidence of high aspect ratio surface structures that are pervasive on Ge surfaces irradiated with higher energy ion beams.[27]

At the beamline, the experimental setup incorporates a custom-built ultrahigh vacuum chamber with a base pressure of 1×10^{-8} Torr. Krypton ions were generated by a Physical Electronics Inc. PHI ion gun set at 1 keV ion energy and using gas of 99.999% nominal purity. The beam diameter was approximately 1.5 cm and the flux during these experiments was approximately 1×10^{12}ions/(cm^2 s) reckoned in a plane perpendicular to the ion beam. Each Ge(001) sample at room temperature was held clipless using silver paste on its backside in the chamber with extra care taken to minimize secondary collisions that might lead to sputtering of material impurities onto the surface. An x-ray flux of approximately 10^{12} photons/s was provided by the National Synchrotron Light Source at beamline X21. A photon wavelength of 0.124 nm was selected by a Si(111) monochromator. The x-ray incidence angle on the sample surface was 0.82° and a 487 × 195-pixel PILATUS area detector[28] measured the scattering pattern.

Figure 1(a) shows the initial GISAXS pattern of a Ge sample with preformed real-space ripples of wavelength 45 nm. Figure 1(b) shows the x direction GISAXS of the same sample after $t = 80$ min bombardment at $\theta = 45°$ incidence. Although the area detector provides both $q_\parallel$ (in-plane) and q_z (out-of-plane) scattering in the GISAXS position, a range of interest corresponding to the Yoneda wing[29] is integrated in the q_z direction for best optimization of surface sensitivity and

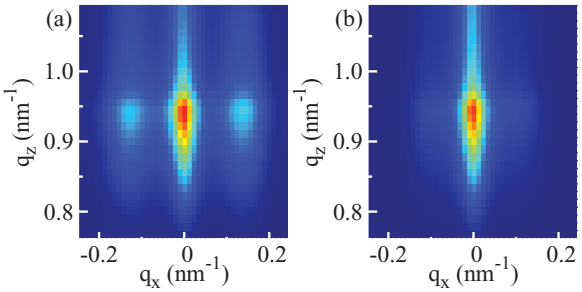

FIG. 1. (Color online) (a) GISAXS area scattering of initially rippled Ge surface. Satellite peaks at $q_x = 0.14$ nm^{-1} correspond to real-space ripple wavelength of 45 nm on the surface. (b) Subsequent GISAXS area scattering of the previous surface after 80 min of Kr^+ ion bombardment at 45° incidence. The satellite peaks are extremely faint, corresponding to a partially smoothed surface.

count rate. Figures 2(a) and 2(c) show examples of the resultant GISAXS time evolution for growth at $\theta = 75°$ in the x direction and smoothing at $\theta = 20°$ in the y direction, respectively. Examples of evolution at typical wave numbers studied with corresponding fits to Eq. (2) are shown in Figs. 2(b) and 2(d). Figures 3(a) and 3(b) show the experimental dispersion relation $R(q_x)$ for ion incidence angles $\theta = 0°$, 20°, 30°, 45°, 55°, 60°, 65°, 70°, and 75° and $R(q_y)$ for angles $\theta = 0°$, 20°, 30°, 45°, 55°, 70°, and 80°.

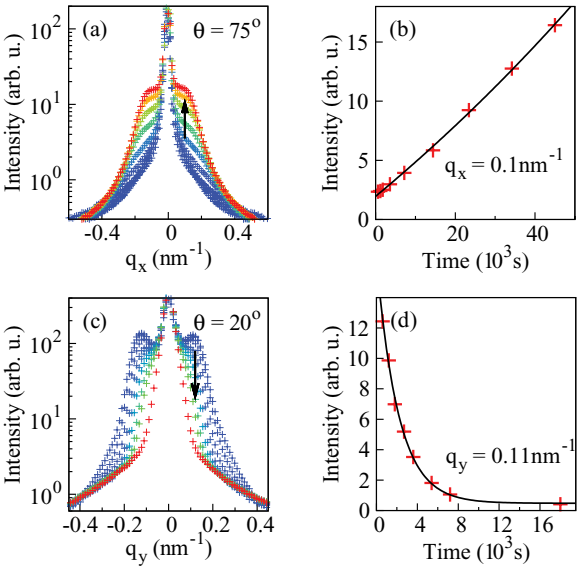

FIG. 2. (Color online) (a) GISAXS *in situ* measurements of pattern formation in the q_x direction during 75° incidence bombardment using an initially smooth surface. Time slices shown from $t = 0$ s to $t = 4.5 \times 10^4$ s, where blue corresponds to earlier times and red to later times. The arrow represents the $q_x = 0.1$ nm^{-1} mode. (b) Corresponding intensity plot showing amplification of one mode $q_x = 0.1$ nm^{-1}, including positive exponential fit. (c) Scattering *in situ* time-slice measurements in the q_y direction showing smoothing during 20° incidence bombardment of an initially rippled surface. Times shown are $t = 0$ s to $t = 1.8 \times 10^4$ s, where blue corresponds to earlier times and red to later times. The arrow represents the $q_y = 0.11$ nm^{-1} mode. (d) Corresponding intensity plot of $q_y = 0.11$ nm^{-1} mode, including exponential fit.

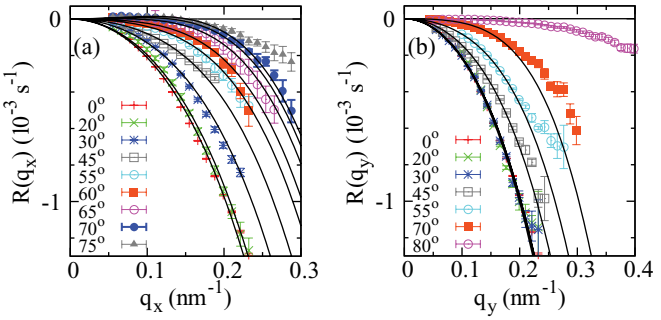

FIG. 3. (Color online) Measured dispersion relations (a) $R(q_x)$ and (b) $R(q_y)$ for a wide range of ion-incidence angles θ, including fits using Eq. (2).

Solid lines in Figs. 3(a) and 3(b) are error-bar-weighted least-square fits of the experimental dispersion relations to Eq. (3), letting $S_x(\theta)$ and $S_y(\theta)$ vary independently for each incidence angle and letting the coefficient B of the quartic term vary as a single angle-independent coefficient for the combined data sets. The y-direction fit at $\theta = 80°$ is excluded because it could not be fit with the same B coefficient as the other data. The value of B that would be necessary to fit the data at $\theta = 80°$ is significantly smaller than the value that fits all the other data. This may suggest that the impact-induced surface-confined viscous flow changes as ion impacts approach grazing incidence, with fewer displacements due to surface channeling and incomplete development of the collision cascade. This tendency is also seen, though to a much lesser extent, in the 70° and 75° x-direction samples, shown in Fig. 3(a), where the high-q data trends to a less negative value than the fits, which is indicative of a smaller value of B. Thus, although the ion-assisted viscous flow coefficient is treated as constant from 0° to 70° ion incidence angle, it apparently decreases as grazing incidence is approached. When excluding the 80° sample and using the rest of the combined data set, the best-fit experimental value is $B = 0.11 \pm 0.01$ nm^4/s. The dispersion relation is negative in the y direction for all samples and also negative in the x direction for ion bombardment range 0°–60°. As seen by the topmost data set in Fig. 3(b), at 80° the dispersion relation at low q_y is small and negative but with error bars that straddle the $R(q) = 0$ line.

The data points in Fig. 4 show the curvature coefficients $S_x(\theta)$ and $S_y(\theta)$ derived from the fits in Fig. 3; these coefficients directly reflect the stability/instability of low-wave-number undulations in the parallel and perpendicular modes, respectively. The y-direction 80° sample is included in Fig. 4 by independently fitting its data for $R(q_y)$, from Fig. 3(b), to Eq. (3) with a different value of B. Figure 4 shows a transition from smoothing to ripple-growth instability in Ge at a critical angle of $\theta_c \cong 62°$. This can be compared with results obtained in a home laboratory using the Veeco RF source with 500 eV bombardment. The transition angle there appears to be slightly below 60°. Whether the small difference between laboratory and synchrotron results is due to the difference in ion energy, difference in source, or difference in geometry is not yet known.

In considering the behavior of $S_x(\theta)$ and $S_y(\theta)$ we begin by recalling the model we had previously used with Ar^+ bombardment of Si to explain the observed kinetics. It is composed of two parts: The erosive component $S^{\text{eros}}(\theta)$ and

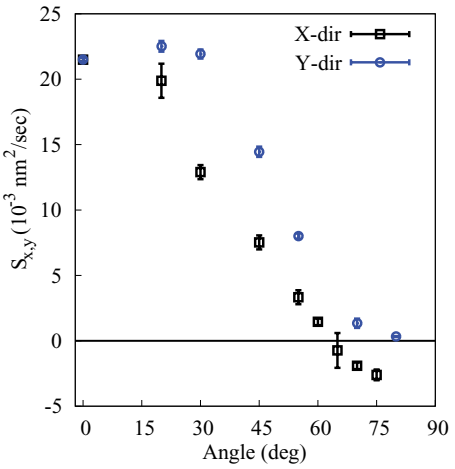

FIG. 4. (Color online) . Best fit results for the curvature coefficient terms as a function of ion incidence angle.

the mass redistributive component $S^{\text{redist}}(\theta)$[17,18,26] as described in Eqs. (5)–(7) of Ref. 24. The experimentally observed $S_x(\theta)$ is clearly positive at low angles, corresponding to a stable surface. This contrasts with the behavior of $S^{\text{eros}}(\theta)$, which is negative at low angles.[17] The redistributive effect switches from stabilizing to causing an instability as θ increases past 45°. The Ge data do show a transition from stability to instability with increasing angle, but the transition angle is approximately 62°. Thus the CV model gives the proper qualitative phase behavior but is not quantitatively accurate. While the simple CV model incorporates no parameters enabling the critical angle to deviate from 45°, the crater function theory of Norris *et al.*[22,23] provides a more general formalism. It takes as input the average change in topography due to a single ion collision event. This can in principle be calculated from molecular dynamics simulations, but such simulations do not currently exist for Kr^+ bombardment of Ge.

In summary, *in situ* GISAXS studies enable us to directly measure the linear dispersion relation $R(\mathbf{q})$ for a wide range of ion incidence angles in both parallel and perpendicular modes, fully characterizing the linear evolution of Ge surfaces during 1 keV Kr^+ ion bombardment at room temperature. The wave number dependence of $R(\mathbf{q})$ is fit well with the sum of a quadratic term determining stability or instability, and a quartic smoothing term. There is a transition at a critical ion incidence angle of $\theta_c \cong 62°$ from stability at lower angles to a parallel-mode instability at higher angles. This transition is qualitatively very similar to that of Si under Ar^+ irradiation and is qualitatively consistent with the behavior expected from the CV lateral mass redistribution model. Quantitatively, however, in contrast to the prior results for Ar^+ bombardment of Si, the value $\theta_c \cong 62°$ for Kr^+ bombardment of Ge cannot be explained by a simple CV redistributive model. Deviations of the lateral mass redistribution away from the simple form assumed by CV, or other effects such as stress, apparently play a significant role.

We thank Alexander DeMasi of B.U. for his help with experiments. We also thank Christie Nelson and Steven LaMarra of Brookhaven National Laboratory at the

National Synchrotron Light Source for their support and help with beamline X21. The B.U. component of this work was supported by NSF DMR-1006538; J.C.P., C.S.M., and M.J.A. were supported by DE-FG-02-06ER46335. Use of the National Synchrotron Light Source, Brookhaven National Laboratory, was supported by the US Department of Energy, Office of Science, Office of Basic Energy Sciences, under Contract No. DE-AC02-98CH10886.

[1]M. Moseler, P. Gumbsch, C. Casiraghi, A. C. Ferrari, and J. Robertson, Science **309**, 1545 (2005).
[2]C. S. Madi, B. Davidovitch, H. B. George, S. A. Norris, M. P. Brenner, and M. J. Aziz, Phys. Rev. Lett. **101**, 246102 (2008).
[3]W. L. Chan and E. Chason, J. Appl. Phys. **101**, 121301 (2007).
[4]G. Ozaydin, A. S. Ozcan, Y. Y. Wang, K. F. Ludwig, H. Zhou, R. L. Headrick, and D. P. Siddons, Appl. Phys. Lett. **87**, 163104 (2005).
[5]G. Ozaydin, K. F. Ludwig, H. Zhou, and R. L. Headrick, J. Vac. Sci. Technol. B **26**, 551 (2008).
[6]G. Ozaydin, K. F. Ludwig, H. Zhou, L. Zhou, and R. L. Headrick, J. Appl. Phys. **103**, 033512 (2008).
[7]J. Zhou and M. Lu, Phys. Rev. B **82**, 125404 (2010).
[8]C. S. Madi, H. B. George, and M. J. Aziz, J. Phys.: Condens. Matter **21**, 224010 (2009).
[9]R. L. Headrick and H. Zhou, J. Phys.: Condens. Matter **21**, 224005 (2009).
[10]D. Carbone, A. Biermanns, B. Ziberi, F. Frost, O. Plantevin, U. Pietsch, and T. H. Metzger, J. Phys.: Condens. Matter **21**, 224007 (2009).
[11]J. A. Sanchez-Garcia, R. Gago, R. Caillard, A. Redondo-Cubero, J. A. Martin-Gago, F. J. Palomares, M. Fernandez, and L. Vazquez, J. Phys.: Condens. Matter **21**, 224009 (2009).
[12]B. Ziberi, Ph.D. Thesis, University of Leipzig, 2006.
[13]B. Ziberi, F. Frost, T. Hoche, and B. Rauschenbach, Phys. Rev. B **72**, 235310 (2005).
[14]B. Ziberi, M. Cornejo, F. Frost, and B. Rauschenbach, J. Phys.: Condens. Matter **21**, 224003 (2009).
[15]Q. Wei, J. Lian, S. Zhu, W. Li, K. Sun, and L. Wang, Chem. Phys. Lett. **452**, 124 (2008).
[16]P. Sigmund, J. Mater. Sci. **8**, 1545 (1973).
[17]R. M. Bradley and J. M. Harper, J. Vac. Sci. Technol. A **6**, 2390 (1988).
[18]G. Carter and V. Vishnyakov, Phys. Rev. B **54**, 17647 (1996).
[19]W. W. Mullins, J. Appl. Phys. **30**, 77 (1959).
[20]C. C. Umbach, R. L. Headrick, and K. C. Chang, Phys. Rev. Lett. **87**, 246104 (2001).
[21]S. E. Orchard, Appl. Sci. Res. A **11**, 451 (1962).
[22]S. A. Norris, M. P. Brenner, and M. J. Aziz, J. Phys.: Condens. Matter **21**, 224017 (2009).
[23]S. A. Norris, J. Samela, L. Bukonte, M. Backman, F. Djurabekova, K. Nordlund, C. S. Madi, M. P. Brenner, and M. J. Aziz, Nat. Commun. **2**, 276 (2011).
[24]E. Anzenberg, C. S. Madi, M. J. Aziz, and K. F. Ludwig Jr., Phys. Rev. B **84**, 214108 (2011).
[25]C. S. Madi and M. J. Aziz, Appl. Surf. Sci. **258**, 4112 (2011).
[26]C. S. Madi, E. Anzenberg, K. F. Ludwig, and M. J. Aziz, Phys. Rev. Lett. **106**, 066101 (2011).
[27]B. R. Appleton, O. W. Holland, J. Narayan, O. E. Schow, J. S. Williams, K. T. Short, and E. Lawson, Appl. Phys. Lett. **41**, 711 (1982).
[28]www.dectris.com.
[29]Y. Yoneda, Phys. Rev. **131**, 2010 (1963).